Design and Control of a Variable Stiffness Actuator for Safe and Fast Physical Human/Robot Interaction

Giovanni Tonietti, Riccardo Schiavi and Antonio Bicchi
Interdepartmental Research Center "E. Piaggio"
Faculty of Engineering, University of Pisa
via Diotisalvi,2 56100, Pisa (Italy)
bicchi@ing.unipi.it

***Abstract*— This paper is concerned with the design and control of actuators for machines and robots physically interacting with humans, implementing criteria established in our previous work [1] on optimal mechanical-control co-design for intrinsically safe, yet performant machines. In our Variable Impedance Actuation (VIA) approach, actuators control in real-time both the reference position and the mechanical impedance of the moving parts in the machine in such a way to optimize performance while intrinsically guaranteeing safety. In this paper we describe an implementation of such concepts, consisting of a novel electromechanical Variable Stiffness Actuation (VSA) motor. The design and the functioning principle of the VSA are reported, along with the analysis of its dynamic behavior. A novel scheme for feedback control of this device is presented, along with experimental results showing performance and safety of a one-link arm actuated by the VSA motor.**

***Index Terms*— Physical Human-Robot Interaction, Safety, Performance, Variable Stiffness Mechanisms, Actuators**

I. Introduction

Machines that interact with humans must be safe against all possible accidents. Taking this for granted, the second most important goal is their performance - which can be often expressed in terms of velocity of motion. A machine that moves fast is typically more dangerous than a slow-moving machine, but slow machines are often unacceptable in applications. Some attempts have been made in the past to overcome this problem by using sensorization of the moving parts of the (rigid) machines, and active control. These solutions tend to be costly, encumbrant, and not sufficiently reliable. A way to mechanically guarantee safety for mechanisms based on passive transmission elasticity has been considered in [2]. More recent approaches include minimization of link and motor inertias, and the design of new transmission mechanisms [3], [4].

A new mechanical/control co–design approach, the Variable Impedance Approach (VIA), has been recently introduced by authors [5] as a new way to optimally trade safety and performance during task executions for a robot arm relying on the possibility to vary the mechanical impedance (i.e. stiffness, damping and/or gear–ratio parameters) of the actuation subsystem "on the fly". In particular, the way in which the mechanical impedance could optimally vary during motions can be determined as a solution of the Safe Brachistochrone optimal control problem introduced by authors in [1]. Results of such analysis show that optimal control of safe VIA mechanisms imposes high stiffness at low link velocities, while low stiffness should be commanded at high velocities, to decouple the actuator's inertia from the link's. Furthermore, the study in [1] shows that a crucial parameter for achieving high performance from VIA mechanism is the ratio between the maximum and minimum achievable actuator stiffness.

It is interesting to note that purposeful variation of impedance is also observed in motions of the human limbs, which appear to be controlled by the cerebellum adopting pre–computed optimal strategies [6]: however, no direct relation has been shown so far between known neural strategies and the strategies resulting from the safe brachistochrone solutions.

The general VIA concept can be implemented by different mechanisms, in particular those adopting antagonistic arrangements emulating human limbs (see e.g. the actuation systems discussed in [7], [8], [9]). However, a broader exploitation of the VIA concept in machines and industrial environments would largely benefit if fast, rugged, and compact VIA actuators were available. To this purpose, this paper discusses the realization of a compact rotary actuator with variable and controllable joint shaft stiffness. Another important issue left open by previous work on VIA actuators and considered here, is their feedback control, to guarantee safety and accuracy in positioning of the mechanism during fast trajectory tracking tasks, in spite of model parameter mismatches or unforeseeable disturbances. Experimental tracking results on both position and stiffness, performed with a prototype of VIA, are reported.

II. Design of a Variable Stiffness Actuator

In this section we present the design of a prototype variable-stiffness actuator (VSA). Although the VSA has been primarily conceived for safe and performant robot arms operating in anthropic environments, it could be also usefully adopted to actuate mechanisms for which the capability to vary stiffness is important during executions of particular tasks (e.g. to better adapt legged robots to various, and unknown conditions of the terrain [10], [11]).

The conceptual design and the appearance of the VSA prototype are described in fig. 1, and 2, respectively . A timing transmission belt, whose total length is $L \approx 0.35$m, is tensioned by springs of elastic constants $K = 3$ N/m,

$K_m = 4$ N/m, and connects nonlinearly the main shaft q_m to the antagonistic pair of actuators pulleys q_1, q_2 rigidly connected to position-controlled backdrivable DC motors. Concordant angular variations $\delta q_1 = \delta q_2$ generate only displacements δq_m at the main shaft, while the opposite $\delta q_1 = -\delta q_2$ generate stiffness variations $\delta\sigma$. Springs of elastic constant K_m on idle pulleys guarantee correct tensioning of the belt. The primary difference between

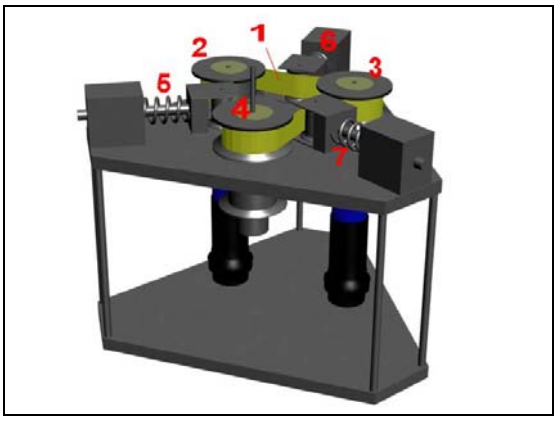

Fig. 1. Perspective view of the Variable Stiffness Actuator. The transmission belt 1 connects the DC Motors pulleys 2-3 to the joint shaft 4, and it is tensioned by passive elastic elements 5-6-7.

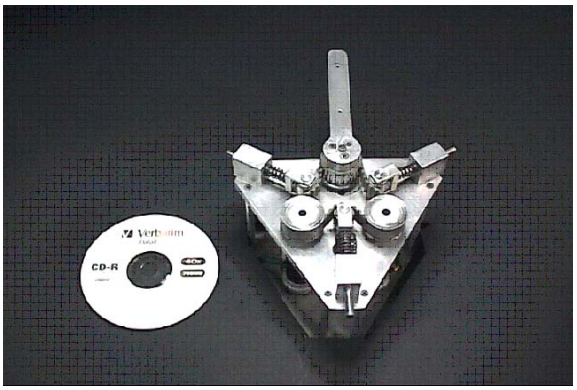

Fig. 2. Appearance of the prototype of Variable Stiffness Actuator.

the proposed transmission system, and other devices with variable mechanical stiffness (see e.g. [12], [13], [7]), is that this is amenable to more compact implementation, and stiffness can be varied very rapidly and continuously during task executions.

To calculate the mechanical stiffness σ of the VSA, we compute the mechanical torque τ generated by the springs of elastic constant K to the joint shaft, and its derivative $\sigma = -\frac{\partial\tau}{\partial q_m}$ with respect to a joint shaft angular displacement q_m. For simplicity, we focus our attention on one of the three sides of the torque transmission system (see fig. 3), calculating the overall torque acting to the joint shaft as the sum of two (i.e. left/right) components. After some calculations, the torque acting on the joint q_b generated by

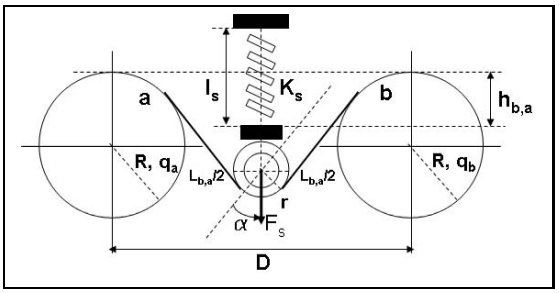

Fig. 3. Particular of the proposed nonlinear torque transmission system. In this case, stiffness $\sigma_{b,a}$ of the belt that connects the two pulleys b, a varies during motions with the active length $h_{b,a}$ of the spring K_s. in such way high/low compressions of the spring generate high/low stiffness.

the spring K_s results

$$\phi_{b,a} = F_{b,a}\cos\alpha R = 2K_s R\frac{\bar{h}_{b,a} - h_{b,a}}{h_{b,a}}L_{b,a},$$

where $L_{b,a} = \hat{L}_{b,a} + R(q_b - q_a)$ is the length of the belt between the two pulleys ($\hat{L}_{b,a} \geq D$ is the length of the belt at the equilibrium), $h_{b,a} = \frac{\sqrt{L_{b,a}^2 - D^2}}{2}$ is the active length of the spring ($\bar{h}_{b,a} \geq h_{b,a}$ represents the spring's length at rest). For simplicity, in these calculations we assumed it holds $r \approx 0$ for the radius of the idle pulley, and that $h_{b,a} \approx l_s$, with l_s is the total length of the spring.

The torque τ acting on the joint shaft of the VSA can be easily computed as

$$\begin{array}{l}\tau = \phi_{m,1} - \phi_{2,m} = \\ 2KR\left(\frac{\bar{h}_{m,1}-h_{m,1}}{h_{m,1}}L_{m,1} - \frac{\bar{h}_{2,m}-h_{2,m}}{h_{2,m}}L_{2,m}\right),\end{array} \quad (1)$$

and the related joint shaft stiffness is

$$\begin{array}{l}\sigma = 2KR\left(\frac{\bar{h}_{m,1}-h_{m,1}}{h_{m,1}} + \frac{\bar{h}_{2,m}-h_{2,m}}{h_{2,m}}\right) - \\ 2KR\left(\frac{\bar{h}_{m,1}L_{m,1}}{4h_{m,1}^3} + \frac{\bar{h}_{2,m}L_{2,m}}{4h_{2,m}^3}\right).\end{array} \quad (2)$$

In fig. 4 are reported values for the VSA's joint stiffness obtained by simulations of (2). As it is highlighted, σ is a monotonically increasing function of the relative displacement $q_d = \frac{q_1 - q_2}{2}$, and it can be shown that angular values $q_1 = -q_2 = \frac{\pi}{2}$ imply for this model $\sigma = +\infty$.

As we will argument in detail in the following, its capability to independently vary its main shaft positions and stiffness highlights the VSA can be usefully adopted to actuate mechanisms for which the characteristic to guarantee safety is of paramount importance during motions [5].

III. Dynamics and Control of VSA systems

In this section we discuss the dynamics and control of a 1-DOF experimental setup constituted by a planar link actuated by the VSA. The proposed control allows to independently vary the position and the stiffness of the joint shaft in a manner that comply to what reported in [1]. Stiffness references will be generated adopting an on–line sub–optimal control algorithm discussed in section III-B. Experimental results are reported in section IV highlighting the effectiveness of the proposed control approach.

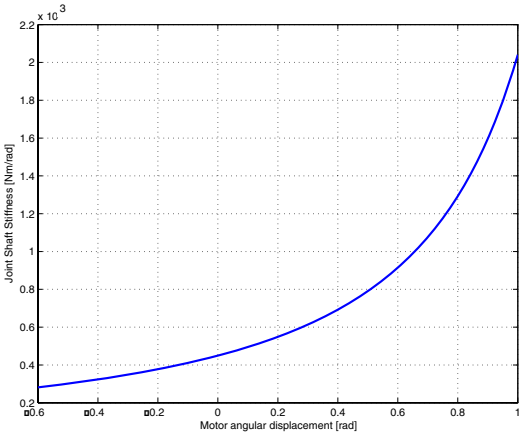

Fig. 4. Values for stiffness σ at the joint shaft of VSA in a steady–state configuration with angular positions $q_m = 0$, and with increasing values for displacements $q_d = \frac{q_1 - q_2}{2}$.

A. Dynamics of the VSA

The appearance of an experimental setup, constituted by a rigid link actuated by the VSA, is reported in fig. 5.

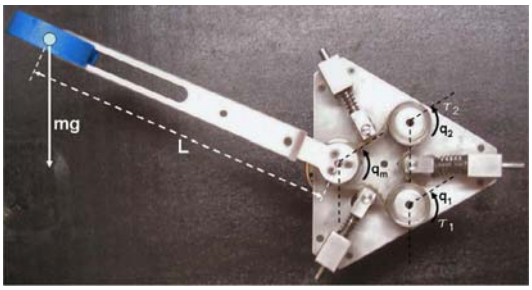

Fig. 5. Appearance of the planar 1-DOF experimental setup realized in our lab.

The dynamics of the system result

$$\begin{cases} I_R\ddot{q}_1 + \beta\dot{q}_1 = \phi_{1,2} - \phi_{m,1} + \tau_1 \\ I_R\ddot{q}_2 + \beta\dot{q}_2 = \phi_{2,m} - \phi_{1,2} + \tau_2 \\ I_L\ddot{q}_m + \beta\dot{q}_m + mgL\sin q_m = \phi_{m,1} - \phi_{2,m} - \tau_m \end{cases} \tag{3}$$

where I_R and I_L are, respectively, the DC motors and link rotary inertias, β is the (small) axial friction coefficient, m and L are the mass and the length of the link, q_1, q_2, q_m are the rotors and link angular positions, $\phi_{1,2}$, $\phi_{2,m}$, $\phi_{m,1}$ are the torques generated on the pulleys by the three springs (see section II), τ_m collects external disturbances acting on the link, and $\tau_{1,2}$ are the control torques acting on the two motors.

The pursued control task is to control the transmission stiffness σ and the joint shaft position q_m by controlling independently the displacements $q_s = \frac{q_1+q_2}{2}$ and $q_d = \frac{q_1-q_2}{2}$. This is suggested by the fact that, in a steady-state configuration, and in presence of negligible gravitational loads (e.g. in case of planar, or lightweight robots, such as those proposed in [3], [14]), for the link angular displacement and transmission stiffness it holds $q_m = q_s$, and $\sigma = \sigma(q_d)$ (see also fig. 6, where transmission stiffness increases from *green* to *red*).

Fig. 6. How stiffness σ varies in practice. Differential displacements $q_d = \frac{q_1 - q_2}{2}$ do not affect the position q_m of the joint shaft, but only the stiffness characteristic of the transmission.

State variables $(q_s,\, q_d,\, \dot{q}_s,\, \dot{q}_d)$ appear on (3) by simply adding and subtracting its first and second equations

$$\begin{cases} I_R\ddot{q}_s + \beta\dot{q}_s = \Phi_s + \tau_s \\ I_R\ddot{q}_d + \beta\dot{q}_d = \Phi_d + \tau_d \\ I_L\ddot{q}_m + \beta\dot{q}_m + mgL\sin q_m = \tau - \tau_m \end{cases} \tag{4}$$

where, in particular, $\Phi_s = \frac{\phi_{2,m} - \phi_{m,1}}{2}$, $\Phi_d = (\phi_{1,2} - \frac{\phi_{2,m} + \phi_{m,1}}{2})$, $\tau_s = \frac{\tau_1 + \tau_2}{2}$, and $\tau_d = \frac{\tau_1 - \tau_2}{2}$ are the respective control torques. Note that torques Φ_s, Φ_d, and $\tau = \phi_{m,1} - \phi_{2,m}$ in (1) are now dependent on variables q_m, q_s, q_d.

An extension of this model to a more general n-DOF structure can be found by supposing the overall system "decoupled" [15], i.e. with Lagrangian function

$$L = \frac{1}{2}\dot{q}^T B_o(q_m)\dot{q} - U_g(q_m) - U_K(q_s, q_d, q_m),$$

where $\dot{q} = (\dot{q}_m, \dot{q}_1, \dot{q}_2)^T$, $B_o(q_m) = \mathrm{diag}[B(q_m), I_R, I_R]$ is a block–diagonal inertia matrix which collects the inertia matrix $B(q_m)$ of the rigid n-DOF structure, and the DC motors rotary inertias I_R of the VSA, $U(q_m)$ is the potential energy of the rigid structure (we supposed to adopt lightweight VSAs, i.e. with negligible gravitational loads), and

$$\begin{aligned} U_K(q_s, q_d, q_m) &= \tfrac{1}{2}K_m(\bar{h}_{1,2} - h_{1,2})^2 \\ &+\tfrac{1}{2}K\left[(\bar{h}_{m,1} - h_{m,1})^2 + (\bar{h}_{2,m} - h_{2,m})^2\right], \end{aligned}$$

is the potential energy stored on the elastic elements of the transmission. Adopting the Lagrange equation, it holds after some calculations

$$\begin{cases} I_R\ddot{q}_s + \beta\dot{q}_s = \Phi_s + \tau_s \\ I_R\ddot{q}_d + \beta\dot{q}_d = \Phi_d + \tau_d \\ B(q_m)\ddot{q}_m + h(q_m, \dot{q}_m) = \tau - J^T(q_m)\tau_m \end{cases} \tag{5}$$

where, in particular, $h(q_m, \dot{q}_m)$ collects Coriolis and gravitational torques acting on the rigid structure, $J(q_m)$ is the Jacobian of the structure, and functions Φ_s, Φ_d, τ, and τ_m

are intended as n-dimensional column vectors collecting the related quantities at each joint.

B. Control of the VSA

Choosing the controls

$$\begin{cases} \tau_s = K_v\dot{\tilde{q}}_s + K_p\tilde{q}_s - \Phi_s \\ \tau_d = K_v\dot{\tilde{q}}_d + K_p\tilde{q}_d - \Phi_d \end{cases} \quad (6)$$

with position errors $\tilde{q}_s = \hat{q}_s - q_s$, $\tilde{q}_d = \hat{q}_d - q_d$ ($\hat{q}_d, \hat{q}_s$ are desired displacements), and both $K_P, K_V > 0$, system (4) results

$$\begin{cases} I\ddot{\tilde{q}}_s + (\beta + K_v)\dot{\tilde{q}}_s + K_p\tilde{q}_s = 0 \\ I\ddot{\tilde{q}}_d + (\beta + K_v)\dot{\tilde{q}}_d + K_p\tilde{q}_d = 0 \\ J\ddot{q}_m + \beta\dot{q}_m + mgL\sin q_m = \\ \phi_{m,1}(q_m, q_s, q_d) - \phi_{2,m}(q_m, q_s, q_d) - \tau_m. \end{cases} \quad (7)$$

In practice an integral term could be added to torques (6) so as to avoid steady–state disturbances, due to the non–perfect modelling of torques $\phi_{m,1}$, $\phi_{2,m}$ affecting the dynamics of variables $\tilde{q}_s$, $\tilde{q}_d$.

The equilibrium point for system (7), with external torque $\hat{\tau}_m$ at the equilibrium, is

$$(\tilde{q}_s, \tilde{q}_d, q_m, \dot{\tilde{q}}_s, \dot{\tilde{q}}_d, \dot{q}_m)^T = (0, 0, \hat{q}_m, 0, 0, 0)^T = \hat{X}$$

with $\hat{q}_m$ is the equilibrium point for the third equation of system (7), i.e. it holds

$$mgL\sin\hat{q}_m - \left(\hat{\phi}_{m,1} - \hat{\phi}_{2,m} - \hat{\tau}_m\right) = 0.$$

To inspect the asymptotical stability of the equilibrium obtained with controls (6), it is sufficient to linearize (7) in proximity of the equilibrium point $\hat{X}$, to obtain

$$\begin{cases} I\ddot{\tilde{q}}_s + (\beta + K_v)\dot{\tilde{q}}_s + K_p\tilde{q}_s = 0 \\ I\ddot{\tilde{q}}_d + (\beta + K_v)\dot{\tilde{q}}_d + K_p\tilde{q}_d = 0 \\ J\ddot{\tilde{q}}_m + \beta\dot{\tilde{q}}_m + \sigma_{\tilde{q}}\tilde{q}_m = \\ = -\sigma_s\tilde{q}_s - \sigma_d\tilde{q}_d - \tilde{\tau}_m. \end{cases} \quad (8)$$

with $\sigma_k|_{k=m,s,d} = -\frac{\partial\phi_{m,1} - \phi_{2,m}}{\partial q_k}|_{\hat{X}}$, and $\sigma_{\tilde{q}} = mgL\cos\hat{q}_m + \sigma_m$ represents the joint stiffness in a steady state configuration which consists of two spring–like contributes of both gravitational torque and transmission system. In absence of transmission (i.e. $\sigma_m = 0$) the link dynamics comply with those of a pendulum, for which the asymptotical stability of an equilibrium is guaranteed only in a portion of the workspace $\hat{q}_m \in (-\frac{\pi}{2}, \frac{\pi}{2})$, i.e. where it holds $mgL\cos(q_m) > 0$ for the gravitational term, or better where stiffness is positive. The presence of a variable stiffness transmission allows to extend the asymptotical stability to the overall workspace, by inserting in parallel to the gravitational spring a spring of elastic constant $\sigma_m > 0$. In fact, the asymptotical stability of the equilibrium is guaranteed in the overall workspace if stiffness $\sigma_{\tilde{q}}$ is always positive, i.e. if a transmission stiffness $\sigma_m > -mgL\cos(\hat{q}_m)$ is chosen.

It is noteworthy to highlight that, in proximity of a steady state equilibrium configuration, in absence of, or with negligible, gravitational loads (i.e. $mgL\cos(q_m) \ll \sigma_m$), it holds for the joint shaft angular displacement

$$\tilde{q}_m = -\frac{\tilde{\tau}_m}{\sigma_m(\hat{q}_s, \hat{q}_d, \hat{q}_m)},$$

that implies the actuator presents a joint shaft stiffness $\sigma = \sigma_m(\hat{q}_s, \hat{q}_d, \hat{q}_m)$ (see fig. 7).

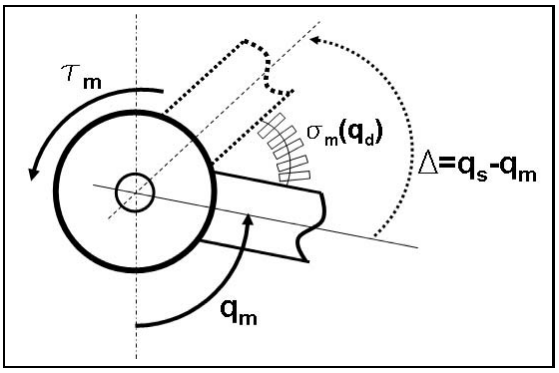

Fig. 7. A simplified working scheme of the VSA in steady–state conditions. Effective q_m, and desired q_s joint displacements are coinciding in case of high transmission stiffnesses $\sigma_m(q_d)$ (i.e. in case of high relative motors displacements q_d), also in presence of external disturbances τ_m.

The latter implies that, for "safe and fast" pick–and–place trajectories in both joint shaft positions and stiffness, such as those computed with the Safe Brachistochrone [1] (see fig. 8), the entity of the position errors $\tilde{q}_m$ decreases while transmission stiffness $\sigma(\hat{q}_s, \hat{q}_d, \hat{q}_m)$ increases (i.e. position errors are negligible during the pick/place intervals).

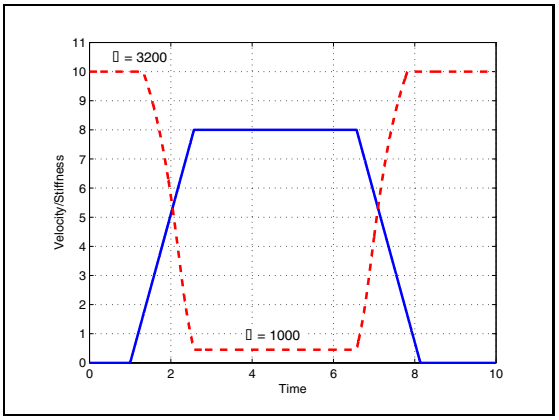

Fig. 8. Trajectories in both joint velocity (*continuous*) and stiffness (*dashed*), for a 1-DOF Soft Arm performing general point–to–point trajectory tracking tasks. Values for transmission stiffness are found as solutions of the Safe Brachistochrone in a manner that leaves the injury level HIC [16] under acceptable safety levels during motion.

IV. Experimental Results

This section is devoted to verify experimentally the performance and intrinsic safety of the controlled prototype in 5. The setup is controlled with methods discussed in section III-B. The capability to independently control joint

shaft position and stiffness proposes the VSA as a viable candidate as actuation system for machines interacting with human operators (see e.g. [5]).

A. Step Responses

The experiment concerns the capabilities of the control approach proposed in section III-B to guarantee the asymptotical stability of the overall system. In particular, in fig. 9 three plots are reported, showing how the steady–state joint shaft position q_m tends to a desired step displacement $\hat{q}_s = \frac{\pi}{2}$, when joint stiffness increases (e.g. $\hat{q}_d = (0, \frac{\pi}{2}, \pi)$).

The latter is a clear effect of the previously discussed properties of disturbance (only gravitational, in this case) rejection of controls (6) for high values of joint stiffness.

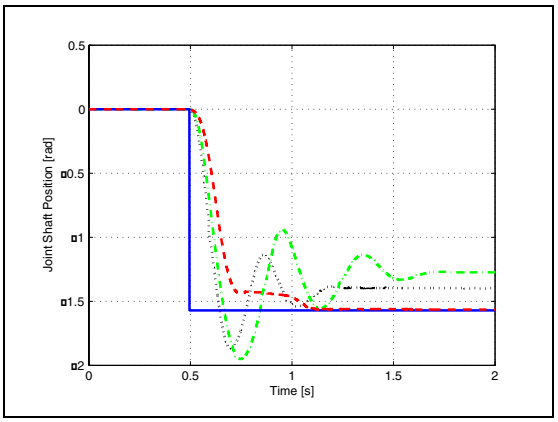

Fig. 9. Step response of the planar experimental setup controlled as in section III-B for desired joint position $\hat{q}_s = \frac{\pi}{2}$ with increasing values for joint stiffness.

B. Trajectory Tracking

This experiment highlights the capabilities of the VSA to vary joint shaft stiffness (see fig. 13) on–line, and independently to general trajectories of the joint shaft (see fig. 12), guaranteeing acceptable levels of HIC [16] during the overall motion. It must be notified that the Safe Brachistochrone is a useful optimal control tool that is able to solve the safety/performance tradeoff in case of point–to–point trajectories (see fig. 8), but, due to his computational complexity, his effectiveness decreases if it is adopted on–line and in presence of general motions.

A low–complexity, sub–optimal, on–line algorithm to guarantee safety during fast motions of the VSA can be conceived directly by inspecting experimental impact results [5], where it can be found that HIC is a monotonic (i.e. invertible) function of transmission stiffness σ_m for constant shaft velocities $\dot{q}_m$ (see fig. 10). The idea is that high transmission stiffnesses $\sigma_m - MAX$ can be preserved without affecting safety during motions until a maximum $\dot{q}_m - MAX$ is reached for the joint shaft velocity, corresponding to a pre–determined maximum level $HIC - MAX$ for injury risk (e.g., in fig. 10, $\dot{q}_m - MAX \approx 5\, m/s$, and $HIC - MAX = 75\, m^{2.5}/s^4$), and hereafter to vary stiffness with velocity along the relative constant–HIC curve, to allow velocity variations without to affect safety (see fig. 11). It is noteworthy that the choice of the "maximum allowable stiffness" which comply with the safety bounds allows the mechanisms to be safe while guaranteeing the maximum allowable accuracy during movements.

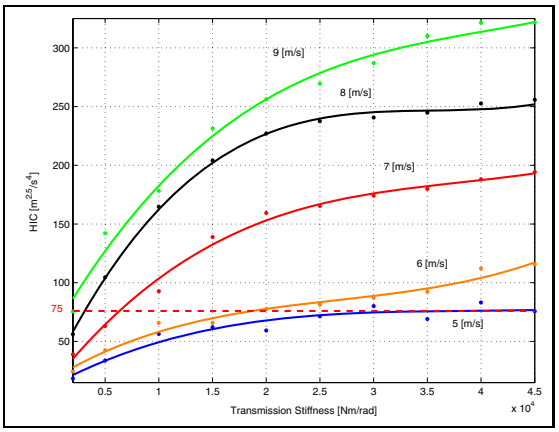

Fig. 10. (HIC experimental results of simulated impacts with the VSA. The dotted line represents the minimum safety level $HIC - MAX = 75\, m^{2.5}/s^4$ allowed during motions.

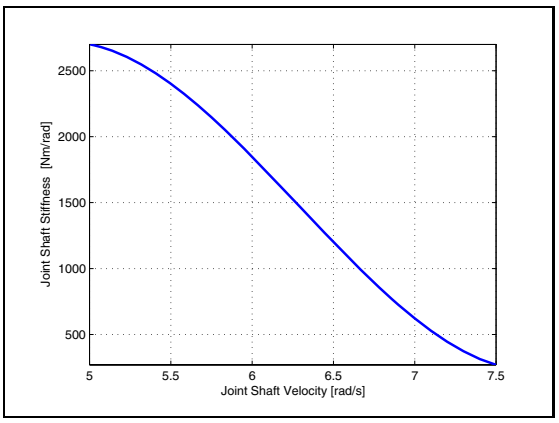

Fig. 11. Constant–HIC curve related to $HIC - MAX = 75\, m^{2.5}/s^4$. Transmission stiffness must vary along this curve for link velocities $\dot{q}_m > 5\, m/s$ to guarantee the safety bound $HIC \leq 75 m^{2.5}/s^4$. The curve has been generated by interpolation of experimental data.

As an example, in case of sinusoidal trajectories $\hat{q}_s$ for the joint shaft (see fig. 12), both desired and experimental values for joint stiffness are reported in fig. 13, where desired trajectories are generated by the T.C.P. [1] to guarantee during motions the safety level $HIC - MAX = 75 m^{2.5}/s^4$. Finally, it can be noticed that, at low velocities, joint shaft positions during the variable stiffness tracking (*continuous*) are practically coincident to those of the rigid case (*dash-dotted*).

This highlights the VIA approach application, in which safety concerns prevail during fast movements, while accuracy in positioning can increase in presence of slow motions.

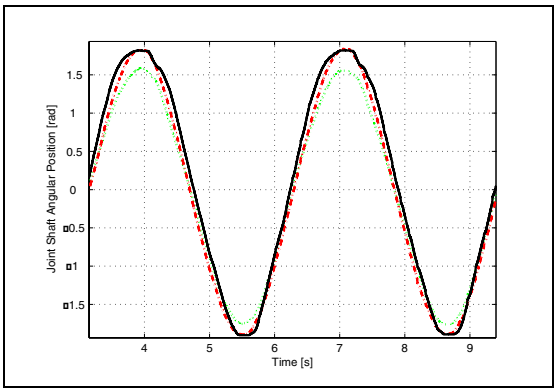

Fig. 12. Trajectory tracking results for a sinusoidal reference, in case of compliant (*dotted*), rigid (*dash-dotted*), and variable stiffness transmission (*continuous*) (see fig. 13 for stiffness trajectories).

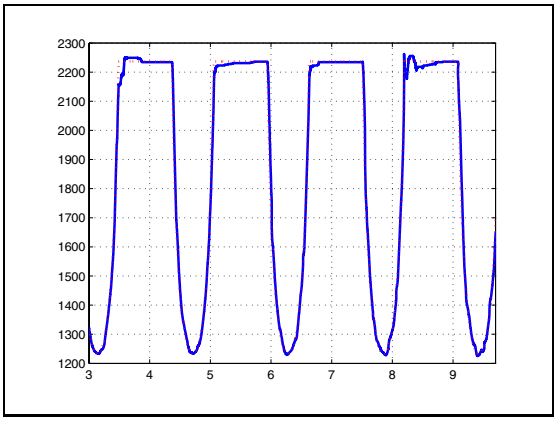

Fig. 13. Stiffness trajectory tracking for the VSA in case of sinusoidal reference at the joint shaft. Desired values for stiffness are computed adopting the sub–optimal algorithm discussed in section IV-B, guaranteeing an $HIC - MAX = 75\, m^{2.5}/s^4$ during the overall motion.

V. Conclusions

In this paper, a Variable Stiffness Actuator is presented in detail, along with a control approach that allows to independently control joint positions and stiffness, and whose effectiveness has been shown both theoretically and experimentally. The possibility to vary transmission stiffness (or impedance, in general) is a useful way to guarantee low levels of injury risk during execution of fast trajectory tracking tasks. That implies the possibility to adopt this actuator to realize fast and safe mechanisms for robotics applications, in which it is involved a close cooperation between human operators and machines.

Acknowledgment

Work partially supported by EC contracts IST-2001-38040 TOUCH-HAPSYS under F.E.T. Presence Initiative and IST-2001-37170 RECSYS. The Variable Impedance Actuation approach, along with its mechanical implementations, has been patented at the Italian Patent Office (Patent No. PI2004A000077). Authors would like to acknowledge the useful help done by Dr. Marco Piccigallo in designing the VSA. Authors would like to gladly acknowledge the quite useful help done by Mr. Fabrizio Vivaldi in building the VSA.

References

[1] A. Bicchi and G. Tonietti, "Fast and soft arm tactics: Dealing with the safety–performance tradeoff in robot arms design and control," *IEEE Robotics and Automation Magazine, Vol. 11, No. 2, June*, 2004.

[2] G. Pratt and M. Williamson, "Series elastics actuators," in *Proc. IEEE/RSJ Int. Conf. on Intelligent Robots and Systems*, 1995, pp. 399–406.

[3] G. Hirzinger, A. Albu-Schäffer, M. Hähnle, I. Schaefer, and N. Sporer, "On a new generation of torque controlled light-weight robots," in *IEEE Int. Conf. on Robotics and Automation*, 2001, pp. 3356–3363.

[4] M. Zinn, O. Khatib, B. Roth, and J. Salisbury, "A new actuation approach for human friendly robot design," in *Proc. of Int. Symp. on Experimental Robotics - ISER'02*, 2002.

[5] G. Tonietti, R. Schiavi, and A. Bicchi, "Optimal mechanical/control design for safe and fast robotics," in *Proceedings of the 9th International Symposium on Experimental Robotics*, Marina Mandarin Hotel, Singapore, 18–21 June 2004.

[6] A. Smith, "Does the cerebellum learn strategies for the optimal time-varying control of joint stiffness?" *Behavioral and Brain Sciences*, vol. 19(3), pp. 399–410, 1996.

[7] J. W. Hurst, J. Chestnutt, and A. Rizzi, "An actuator with mechanically adjustable series compliance," Robotics Institute, Carnegie Mellon University, Pittsburgh, PA, Tech. Rep. CMU-RI-TR-04-24, April 2004.

[8] A. Bicchi and G. Tonietti, "Design, realization and control of a passively compliant robot for intrinsic safety," in *Proc. Second IARP/IEEE–RAS Joint Workshop on Techical Challenge for Dependable Robots in Human Environments*, 2002.

[9] K. F. Laurin-Kovitz, J. E. Colgate, and S. D. R. Carnes, "Design of programmable passive impedance," in *Proc. IEEE Int. Conf. on Robotics and Automation*, 1991, pp. 1476–1481.

[10] H. Kimura and Y. Fukuoka, "Towards adaptive walking of quadruped robot in outdoor environment based on biological concepts," in *Proceedings of the 9th International Symposium on Experimental Robotics*, Marina Mandarin Hotel, Singapore, 18–21 June 2004.

[11] H. Quiang, K. Yokoi, S. Kajita, K. Kaneko, H. Arai, N. Kovachi, and K. Tanie, "Planning walking patterns for a biped robot," *IEEE Transaction on Robotics and Automation*, vol. 11, no. 3, pp. 280–289, June 2001.

[12] M. Okada and Y. Nakamura, "Development of the cybernetic shoulder - a three-dof mechanism that imitates biological shoulder motion," in *Proc. IEEE/RSJ Int. Conf. on Intelligent Robots and Systems*, 1999, pp. 453–548.

[13] T. Morita and S. Sugano, "Development and evaluation of seven d.o.f. mia arm," in *Proc. IEEE Int. Conf. on Robotics and Automation*, 1997, pp. 462–467.

[14] A. Albu-Schäffer and G. Hirzinger, "Cartesian compliant control strategies for light-weight, flexible joint robots," in *Contro l Problems in Robotics*, ser. Springer Tracts in Advanced Robotics - STAR, A. Bicchi, H. Christenses, and D. Prattichizzo, Eds. Springer-Verlag, Berlin, 2003, vol. 4.

[15] M. Spong, "Modeling and control of elastic joint robots," *ASME Journal of Dynamic Systems, Measurement, and Control*, vol. 109, no. 4, pp. 310–319, 1987.

[16] J. Versace, "A review of the severity index," in *Proc. of the Fifteenth Stapp Car Crash Conference*, no. SAE Paper No. 710881. Society of Automotive Engineers, 1971, pp. 771–796.